Simulation of Low Pressure Plasma Processing Reactors: Kinetics of Electrons and Neutrals

R. R. Arslanbekov and V. I. Kolobov

CFD Research Corporation, Huntsville, AL, USA

Abstract. In this paper, we illustrate different aspects of electron kinetics and rarefied gas effects in low pressure inductively coupled plasmas (ICPs). We focus on deterministic methods of solving the Boltzmann equation and its derivatives. Due to small electron mass, the Boltzmann equation for electrons can be reduced to a Fokker-Planck equation of lower dimensionality and solved together with electromagnetic and continuum flow equations for a self-consistent modeling of the plasma. The ions can be described by the so-called ion-momentum equations and the transport of neutral species is described by the traditional Navier-Stokes (NS) solver. This model is used in the CFD-ACE-Plasma code. We apply this code to model ICPs. The transport of neutral species is also simulated using the Unified Flow Solver (UFS). The UFS code uses coupled kinetic or continuum solvers based on appropriate continuum breakdown criteria. The Boltzmann equation is solved in the kinetic domains and the kinetically consistent NS solver is used in the continuum domains. The non-uniform heating of the reactor results in vortex gas flow driven by the solid surface temperature gradients. Significant flow velocities are predicted which can modify distributions of active radicals in the plasma volume and hence can be of importance for modeling the semiconductor processing devices at low gas pressures. This flow is absent in simulations based on the traditional NS solvers with velocity and temperature slip boundary conditions. The correct description of this phenomenon requires application of the kinetic methods.

Keywords: kinetics of electrons and neutral species, low-pressure gas discharges, plasma simulations, semiconductor processing.
PACS: R51.10.+y, 52.65.-y,

INTRODUCTION

Low-pressure plasma processing reactors used in modern semiconductor manufacturing frequently operate in a transitional regime, at Knudsen numbers $Kn = 0.1–1$ both for electrons and neutral (or charged) heavy particles. The electron kinetics is well known to play a very important role in these reactors and it defines the key properties of the weakly ionized plasma including the rates of electron induced chemical reactions. The transport and chemistry of neutral and charged heavy species determine the spatial distributions of active radicals responsible for etch/deposition processes. In the transitional regime, rarefied gas effects are significant and continuum models might be unreliable. Non-uniform gas heating induces temperature-driven flows that could affect uniformity of different processes across the semiconductor wafer. A coupled nature of plasma and rarefied gas phenomena makes it difficult to develop adequate kinetic models of these systems, attempts to use the particle codes are described in [1].

In this paper, we illustrate different aspects of electron kinetics and rarefied gas effects in low pressure inductively coupled plasmas. We focus on deterministic methods of solving the Boltzmann equation and its derivatives. Due to small electron mass, the Boltzmann equation for electrons can be reduced to a Fokker-Planck equation of lower dimensionality and solved together with electromagnetic and continuum flow equations for a self-consistent modeling of electron kinetics and electromagnetics [2]. In currentless plasmas such as ICP, most electrons are trapped in plasma by the ambipolar electrostatic potential. At low gas pressures, they collide more frequently with the potential barrier itself than with neutral particles. Stochastic electron heating, anomalous skin effect and other collisionless phenomena become important under these conditions. Together with the electron distribution function and spatial distribution of charged and neutral species, self-consistent plasma simulations provide the spatial distribution of the reactor temperature. This approach is realized in the CFD-ACE-Plasma code [3].

More accurately, the transport of neutral species can be simulated using the Unified Flow Solver (UFS) developed in [4]. The UFS uses kinetic or continuum solvers based on appropriate continuum breakdown criteria. The Boltzmann equation is solved in the kinetic domains and the *kinetically consistent* Navier Stokes (NS) solver is used in the continuum domains. The non-uniform gas heating in the reactor results in vortex flow driven by the temperature gradients. This flow is absent in simulations based on the *traditional* NS solvers as pointed out by Sone [5]. To our knowledge, this kinetic "ghost effect" which manifests itself even in near-continuum regimes has been neglected in simulations of low-pressure plasma reactors. Deterministic Boltzmann solvers have clear advantages over DSMC for simulations of low speed flows driven by temperature gradients. We will present results of our studies of the importance of these rarefied gas effects in plasma processing reactors.

PARTICLE KINETICS OF WEAKLY-IONIZED PLASMAS

The weakly-ionized plasma is a quasi-neutral mixture of electrons, ions and neutral particles. At kinetic level, each component is described by a kinetic equation for the particle distribution function $f_\alpha(\mathbf{r},\mathbf{v},t)$

$$\frac{\partial f_\alpha}{\partial t} + \nabla_{\mathbf{r}}\cdot(\mathbf{v}f_\alpha) + \nabla_{\mathbf{v}}\cdot(\mathbf{a}f_\alpha) = I_{\alpha\beta} \tag{1}$$

Here **r** is a position vector in physical space, **v** is the velocity vector, **a** is the acceleration vector and *t* is time. The right hand side of Eq. (1) describes binary collisions among particles. Consider for simplicity the simplest case of a three-component plasma consisting of electrons, positive ions and neutral atoms $\alpha,\beta = e,i,n$.

Electrons

For electrons, elastic collisions with neutrals usually dominate over collisions among charged particles. Due to disparity of electron/atom mass ($m/M \ll 1$), the Boltzmann collision integral for elastic collisions of electrons with heavy neutrals can be written in the so-called Lorentz-gas form:

$$I_{en}^{el} = -\frac{1}{\upsilon^2}\frac{\partial}{\partial\upsilon}\upsilon^2\Gamma - N\upsilon\int_{S^2}\sigma(\upsilon,|\Omega-\Omega'|)\left[f(\upsilon,\Omega')-f(\upsilon,\Omega)\right]d\Omega' \tag{2}$$

where Ω is the velocity angle on a unit sphere S^2 in velocity space ($\mathbf{v} = \upsilon\Omega$) and σ is the collision cross section, and *N* is the gas density. The flux Γ is given by

$$\Gamma = -\frac{\delta\nu}{2}\left(\upsilon f + \frac{T}{m}\frac{\partial f}{\partial\upsilon}\right), \tag{3}$$

where *T* is the gas temperature, ν is the transport collision frequency and $\delta = 2m/M$ is the average fraction of the energy lost by the electrons in one elastic collision. The first term in Eq. (3) is small and describes energy exchange between electrons and neutrals. The second, leading term in Eq. (3) describes collisions with infinitely heavy particles which tend to isotropize the electron distribution but do not change their energy. Thus, due to mass disparity, electron momentum relaxation in elastic collisions occurs much faster than energy relaxation, and the EDF averaged over velocity angles, f_0, evolves on a time scale $\tau_u \sim \tau M/m$ which is much slower than evolving the complete distribution. Inelastic processes do not change this picture if characteristic energy of electrons is small compared to the inelastic threshold [6].

For collisional or weakly collisional plasmas, a two-term spherical harmonics expansion of the EDF in velocity space with $f(\mathbf{r},\mathbf{v},t) = f_0(\mathbf{r},\upsilon,t) + \frac{\mathbf{v}}{\upsilon}\cdot\mathbf{f}_1(\mathbf{r},\upsilon,t)$ is commonly used, in which the 6D Boltzmann equation is reduced to a set of two 4D (3D in physical space and 1D in velocity/energy space) equations:

$$\frac{\partial\mathbf{f}_1}{\partial t} + \nu_m\mathbf{f}_1 = -\upsilon\nabla f_0 - \frac{e\mathbf{E}}{m}\frac{\partial f_0}{\partial\upsilon} \tag{4}$$

$$\frac{\partial f_0}{\partial t} + \frac{\upsilon}{3}\mathrm{div}(\mathbf{f}_1) + \frac{1}{3\upsilon^2}\frac{\partial}{\partial\upsilon}\left(\upsilon^2\frac{e\mathbf{E}}{m}\cdot\mathbf{f}_1\right) = S_0\,. \tag{5}$$

Further simplification is possible for collisional plasmas by neglecting electron inertia and introducing the so-called total electron energy $\varepsilon = u - e\phi(\mathbf{r},t)$ with ϕ being the electric potential. The kinetic equation for the electron energy probability function (EEPF) f_0 can then be written in the form (e.g., [13])

$$\frac{\partial f_0}{\partial t} - \frac{\partial \phi}{\partial t}\frac{\partial f_0}{\partial \varepsilon} - \nabla \cdot D_r \nabla f_0 + \frac{1}{\chi}\frac{\partial}{\partial \varepsilon}\left(\chi \left[D_\varepsilon(\mathbf{r},\varepsilon)\frac{\partial f_0}{\partial \varepsilon} + V_\varepsilon(\mathbf{r},\varepsilon) f_0 \right] \right) = S\,, \tag{6}$$

where $u = m\upsilon^2/2e$ is the volt-equivalent of the kinetic energy. Eq. (6) describes the diffusion in physical space (second term), with a diffusion coefficient $D_r = \upsilon^2/3\nu$, the heating due to external electromagnetic fields and quasi-elastic processes represented by the diffusion and convection along the energy axis with a convection velocity V_u and a diffusion coefficient in energy D_u. The quasi-elastic processes include elastic collisions of electrons with neutrals, excitation of molecular vibrations, Coulomb interactions among electrons and ions, and electron heating by electromagnetic fields. Strongly inelastic collisions (excitation, ionization, attachment, etc.) are described the term *S* in Eq. (6). Specific expressions for *S* and $\delta(u)$ can be found, for instance, in [7]. Eq. (6) is solved in a coupled manner with the Poisson equation, the electromagnetic, chemistry, heat and other modules in the CFD-ACE-Plasma code (see e.g., [8]).

Ions

For ions, the main types of collisions are elastic collisions with neutral atoms and charge exchange collisions with parent gas atoms. The typical ion distribution function in collisional plasma is a shifted Maxwellian distribution with drift velocity υ_{dr} exceeding the thermal velocity υ_{th}. In particular, at the plasma sheath boundary, the mean drift velocity of ions is equal to the Bohm velocity $\upsilon_B = \sqrt{T_e/T_i}\,\upsilon_s$ where υ_s is the sound velocity. Thus, the ions enter the sheath with a supersonic velocity. If charge exchange collisions dominate (ions moving in a parent gas) the ion distribution is strongly anisotropic and extends along the field direction from 0 to υ_{dr}, whereas it is only from 0 to υ_{th} in the other direction. The ion-momentum equations are used in the CFD-ACE-Plasma code to model ions.

Neutrals

Collisions among neutral atoms tend to Maxwellize the velocity distribution of neutrals, collisions with electrons and ions result in momentum and energy transfer from charged particles to neutrals. The conventional Navies-Stocks equations are solved in CFD-ACE-Plasma package to model the transport of neutrals. The kinetics of neutral species become import for higher Knudsen numbers *Kn* which are realized in low pressure plasma processing reactors and some effects require kinetic solvers to be properly described. In addition, fast neutrals are produced in charge exchange collisions with energetic ions, especially near the plasma boundaries (plasma sheathes). These fast (non-thermalized) neutrals could be important for gas heating effects [9] and for the plasma processing applications. These effects must be described using the kinetic approach [9].

SIMULATION RESULTS

We demonstrate here typical results of 2D self-consistent simulations of ICP for experimental system studied in details by Godyak's group over the last several years (see [10] and [11] and references therein). The experimental setup and electrical characteristics of this system are described in details in [10]. The plasma is created in a cylindrical chamber of radius *R* = 10 cm and length *L* = 10.5 cm driven by a planar 5-turn coil separated from dielectric (quartz) window by a Faraday shield. With good accuracy, the system is axially symmetric and 2D simulations are sufficient. Experimental data for this system were described in [11] for a wide range of operating conditions, pressure 0.3−100 mTorr, power absorbed in plasma 12−400 W and driving frequency 0.45−13.56 MHz. Such systems can operate at large power inputs and significant reactor heating can occur. Figure 1 (left) shows a typical distribution of the calculated power deposition and schematics of the studied ICP reactor for 10 mTorr, 6.8 MHz and 400 W. Figure 1 (right) shows distribution of the temperature in the whole reactor volume (including the quartz windows and air volume). One can see that at 400 W of input power there is significant heating of the reactor gas and walls. The predicted gas temperature of 480 K at the discharge center is very close to that of about 490 K estimated experimentally in [11]. Heating of gas and reactor walls has been experimentally observed to affect the

plasma parameters in ICP even at more moderate input powers [11]. Non-uniform gas and reactor heating occurs due to ion and electron collisions with neutrals in the bulk plasma and heat release at surfaces due to ion bombardment and surface reactions. Figure 2 (left insert) shows results of calculations of the gas temperature as a function of input power for three different operating pressures. The overall picture presented in Figure 2 is very similar to that estimated in [11]. The heating of the gas in the plasma volume has many important consequences among which is local reduction of gas density (increase of the mean free paths). Another important consequence is that due to the non-uniform temperature of the walls (in this case, the quartz wall), there can arise temperature induced gas flow. This flow can affect distribution of active species in the plasma volume and on the wafer surface. This is discussed in the following section.

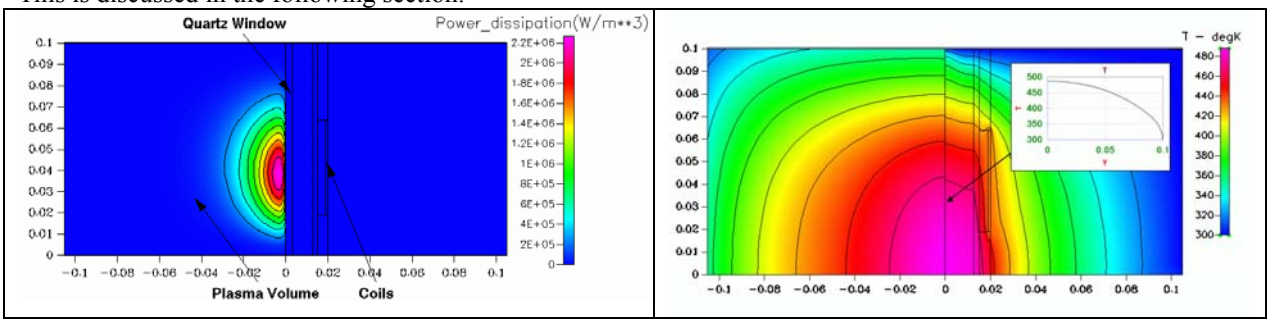

FIGURE 1. Left: calculated power deposition and schematics of ICP reactor for 10 mTorr, 6.8 MHz and 400 W. Right: calculated reactor temperature for these conditions with the wall temperature along the quartz window surface in the insert.

The measured [12] and calculated EEPF are shown in Figure 2 (right) as functions of total electron energy at different points along the discharge axis at radius $r = 4$ cm where the induced electric field reaches maximum value. It is seen that the body of the EEPF depends solely on total electron energy and the EEPF tail is enhanced by hot electrons near the coil due to electron heating, in accordance with the experiments. Similar results were obtained for a different system in a series of publications by Kortshagen and his colleagues (see [13], [14], and [15]) using the same computational approach and by Vasenkov & Kushner [16] using Monte Carlo model for electrons.

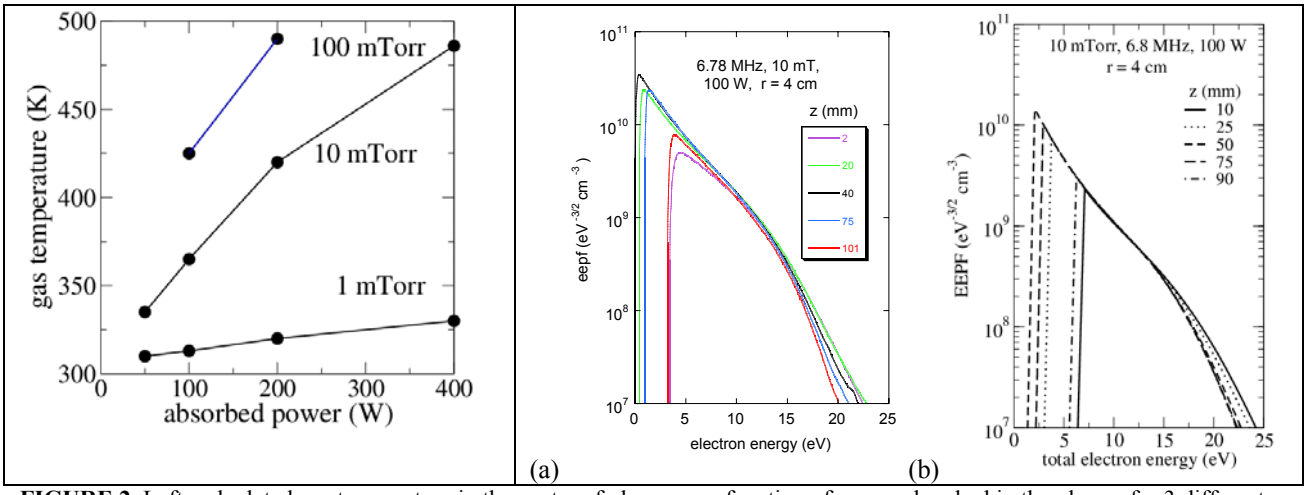

FIGURE 2. Left: calculated gas temperature in the center of plasma as a function of power absorbed in the plasma for 3 different pressures. Right: experimental (a) and calculated (b) electron energy probability function at different points along the discharge axis at a radial position $r = 4$ cm.

SOLID SURFACE TEMPERATURE INDUCED GAS FLOW IN PLASMA PROCESSING REACTORS

The significant power inputs in the plasma reactors results in heating of the gas and of the reactor walls. The fact that the solid surface temperature is different can result in gas flow from colder to hotter regions. As has been recently pointed out in [17], this effect can be of importance for microfluidics. In the present work, we demonstrate its relevant importance for low-pressure plasma reactor simulations. As discussed by Sone [5] (in relation to the so-called "ghost" effect), the traditional NS equations with the velocity and temperature slip boundary conditions in this

case give zero flow velocity and symmetric distribution of gas temperature (in the absence of buoyancy effect due to gravitational forces). For example, the following velocity and temperature slip boundary conditions are used in the CFD-ACE with a conventional NS solver

$$u_s = \lambda \frac{2-\alpha}{\alpha}\left(\frac{\partial u_x}{\partial n}\right)_{wall} \quad \text{and} \quad T_s = T_{wall} - 2\lambda \frac{2-\alpha}{\alpha}\left(\frac{\partial T}{\partial n}\right)_{wall}, \tag{7}$$

where u_s is the tangential slip velocity, α is the (momentum or energy) accommodation coefficient, λ is the mean free path and x is the tangential coordinate to the wall and n is the normal to the wall. The CFD-ACE code predicts zero-flow solutions. In order to predict the phenomenon of thermal-stress slip flow in the framework of the traditional NS approach, the Maxwell-Burnett boundary condition should be used [17]. The simple scalar form of this boundary condition reads (see [17] for details)

$$u_s = \lambda \frac{2-\alpha}{\alpha}\left(\frac{\partial u_x}{\partial n}\right)_{wall} + \frac{3}{4}\frac{\mu}{\rho T}\frac{\partial T}{\partial x}, \tag{8}$$

where μ is the gas viscosity and ρ is the gas density. In the kinetically consistent NS solvers, on the other hand, one can directly set the diffuse reflection boundary condition in terms of reflected half-fluxes based on the values of the surface temperature. This allows one to predict this flow naturally, without using some specially derived boundary conditions. To demonstrate this, we use UFS to solve this problem. The examples of calculation of the velocity flow field distributions by the kinetic NS solver (part of UFS) for 3 Knudsen numbers of 0.01, 0.06 and 0.3 are shown in Figure 3. The temperature of the right wall is approximated by that obtained by the CFD-ACE-Plasma code (see insert in Figure 1 right) and that of the left and top walls is set to 1, with the bottom boundary being symmetry. One can see the temperature induced vortex flow in the middle of the reactor volume. The maximum velocity amplitude of 0.007 of the thermal velocity is obtained at $Kn \sim 0.1$. This means that for these conditions, the flow speed of about 2 m/s can be realized which is comparable with or larger than typical gas flow speeds at reactor inlets. We observed that the induced flow speed is maximum at some Kn (here, ~ 0.1) with the flow speed becoming small at free molecular flow conditions ($Kn = \infty$) and at purely continuum conditions ($Kn = 0$). We also note that we have carried out simulations of the "ghost" effect under conditions used by Sone [5] and obtained good agreement with his linearized Boltzmann equation calculations. We also used the full Boltzmann solver (both with hard sphere and BGK collisional operators) and obtained close results to those of the kinetic NS solver (see also [18]).

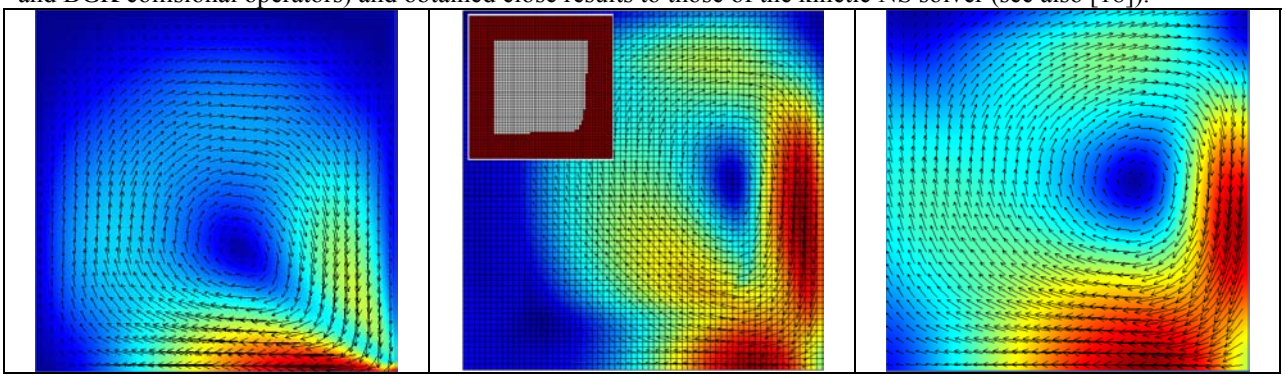

FIGURE 3. Flow velocity vector field and velocity amplitude $|\upsilon|$ distribution for 3 Knudsen numbers: $Kn = 0.01$ (maximum velocity $|\upsilon|_{max} \sim 0.0005$) calculated with the kinetic NS solver, $Kn = 0.06$ ($|\upsilon|_{max} \sim 0.007$) calculated with UFS (kinetic region is shown in red in the insert) and $Kn = 0.3$ ($|\upsilon|_{max} \sim 0.005$) calculated with the Boltzmann solver.

CONCLUSIONS

We have carried out simulations of an ICP reactor at low gas pressures using the CFD-ACE-Plasma code and obtained good agreement with experimental measurements of plasma parameters (the electron distribution function, charged and neutral density and temperature) and gas temperature estimates. The code incorporates a kinetic solver for electron transport and a conventional NS solver for transport of neutral species. Using the UFS code, which incorporates the kinetic NS and Boltzmann solvers, we have carried out computations of the transport of neutrals in a low pressure ICP reactor using the wall temperature distributions obtained by the CFD-ACE-Plasma code. We show that due to non-uniformity of the reactor wall temperature, vortex flows are induced under typical operating conditions. Significant flow velocities are obtained, which can affect the distributions of active radicals in industrial

plasma reactors. This effect of temperature induced flow is missing altogether in the conventional NS computations with standard boundary conditions. In order to capture this effect, the transport of neutral species has to be described by using kinetic methods or by using the boundary conditions based on kinetic considerations.

ACKNOWLEDGMENTS

This work is supported in part by the US Air Force SBIR Project F33615-03-M-3326. The profound expertise in kinetic theory of gases of Dr. Anna Frolova, Prof. Vladimir Aristov and Dr. Sergey Zabelok is gratefully acknowledged. Thanks are due to Mr Eswar Josyula for useful discussions and guidance and Dr A. Singhal for support.

REFERENCES

1 K. Nanbu, *Particle modeling of noneqilibrium plasmas and gases for materials processing*, Recent Res. Devel. Vacuum Sci. Tech. (Transworld Research Network, Kerala, India), **5,** 1-57 (2004).
2 V. I. Kolobov and R. R. Arslanbekov, *Simulation of electron kinetics in gas discharges*, IEEE Trans. Plasma Science, **34**, 895 (2006).
3 CFD Research Corporation, *CFD-ACE+ Module Manual* (http://www.cfdrc.com/bizareas/matls_proc/plasma/).
4 V. I. Kolobov, R. R. Arslanbekov, V. V. Aristov, A. A. Frolova, and S. A. Zabelok, J. Comp. Phys. (submitted).
5 Y. Sone, *Kinetic Theory and Fluid Dynamics*, Birkhauser, Boston, 2002.
6 V. P. Vstovsii, *Kinetics of a weakly ionized plasma in external field*, Sov. J. Plasma Phys. **12**, 856 (1986).
7 L. M. Biberman, V. S. Vorob'ev and I. T. Yakubov, *Kinetics of Nonequilibrium Low-Temperature Plasmas*, Springer (1987).
8 R. R. Arslanbekov and V. I. Kolobov, *Two-dimensional simulations of the transition from Townsend to glow discharge and subnormal oscillations*, J. Phys. D. **36**, 2986 (2003).
9 R. R. Arslanbekov, *Model of the cathode region and gas temperature of a dc glow discharge at high current density*, J. Phys. D: Appl. Phys. **33**, 524 (2000).
10 V. A. Godyak, R. B. Piejak and B. M. Alexandrovich, *Experimental setup and electrical characteristics of an inductively coupled plasma*, J. Applied Phys. **85**, 703 (1999).
11 V. A. Godyak, R. B. Piejak and B. M. Alexandrovich, *Electron energy distribution function measurements and plasma parameters in inductively coupled argon plasma*, Plasma Sources Sci. Technol. **11**, 525 (2002).
12 V. A. Godyak, *Nonequilibrium EEDF in Gas Discharge Plasmas*, IEEE Trans. Plasma Science, **34**, 755 (2006).
13 U. Kortshagen, I. Pukropski and L. D. Tsendin, Phys Rev E **51**, 6063 (1995).
14 G. Mumken, *Spatial profiles of a planar inductively coupled discharge in Argon*, J. Phys D **32**, 804 (1999).
15 U. Kortshagen and B. Heil, *Kinetic modeling and experimental studies of large scale low pressure RF discharges*, J. Tech. Phys. **41**, 325 (2000).
16 A. V. Vasenkov and M. J. Kushner, *Electron energy distributions and anomalous skin depth effects in high plasma density inductively coupled discharges*, Phys. Rev. E **66**, 066411 (2002).
17 D. A. Lockerby, J. M. Reese, D. R. Emerson and R. W. Barber, *Velocity boundary condition at solid walls in rarefied gas calculations*, Phys. Rev. E **70**, 017303 (2004).
18 V. V. Aristov, A. A. Frolova, S. A. Zabelok, V. I. Kolobov and R. R. Arslanbekov, *Simulations of Low Speed Flows with Unified Flow Solver*, RGD25 Proceedings.